CrystEngComm

Cite this: *CrystEngComm*, 2012, **14**, 492

www.rsc.org/crystengcomm

PAPER

Formate modulated solvothermal synthesis of ZIF-8 investigated using time-resolved *in situ* X-ray diffraction and scanning electron microscopy†

Janosch Cravillon,*[a] Christian A. Schröder,[a] Helge Bux,[b] André Rothkirch,[c] Jürgen Caro[b] and Michael Wiebcke*[a]

Received 4th August 2011, Accepted 29th September 2011
DOI: 10.1039/c1ce06002c

Time-resolved investigations using *in situ* energy-dispersive X-ray diffraction in tandem with *ex situ* scanning electron microscopy revealed that solvothermal crystallisation of ZIF-8 in methanol solvent and in the presence of sodium formate as a simple monodentate ligand (modulator) is a rapid process yielding big, high-quality single crystals in short time (<4 h). Kinetic analysis of crystallisation curves was performed by applying the Avrami–Erofe'ev and Gualtieri models. The analyses revealed that the weakly basic formate modulator acts as a base in deprotonation equilibria (deprotonation of the bridging 2-methylimidazole ligand) rather than as a competitive ligand in coordination equilibria at the metal (Zn^{2+}) centres. This is in contrast to the coordination modulation function of formate in ZIF-8 synthesis at room temperature. Crystal shape evolves with time in the presence of formate from cubes with truncated edges to rhombic dodecahedra. The latter shape represents most likely the stable equilibrium morphology of ZIF-8.

Introduction

Zeolitic imidazolate framework (ZIF) materials[1] constitute a novel distinctive subclass of crystalline porous coordination polymers (PCPs) or metal–organic frameworks (MOFs).[2] The three-dimensional framework structures of ZIFs are formally obtained from those of aluminosilicate zeolites by replacement of the tetrahedral Al/Si centres and bridging O atoms by divalent metal cations (M = Zn, Co) and substituted imidazolate anions (im), respectively. Similarity of the angles sustained at the Al–O–Si and M–im–M bridges (~145°) gives rise to topological related tetrahedral networks. For example, ZIF-8 of composition $[Zn(mim)_2]\cdot nG$ (Hmim = 2-methylimidazole, G = guest) crystallises with a cubic sodalite-related framework.[3] Recent research has revealed that ZIFs are very promising materials for many applications in fields such as gas storage,[4] separation,[5] catalysis[6] and sensing.[7]

However, to tune ZIFs for particular applications, methods have to be developed that enable the controlled synthesis of crystals with well-defined size and shape.[8] To reach this goal our current understanding of the crystallisation processes has to be significantly improved,[9] although recent time-resolved investigations using static light scattering (SLS),[10] small-angle and wide-angle X-ray scattering (SAXS/WAXS),[11] and transmission electron microscopy and X-ray diffraction (TEM/XRD)[12] have provided first insight into ZIF-8 nucleation and growth at room temperature by revealing the occurrence of transient clusters, nanoparticles and nanocrystals.

A very attractive method to control size and shape that has been recently introduced to prepare carboxylate-based MOF crystals from the nanoscale to the macroscale is the coordination modulation method.[13–15] An auxiliary monodentate carboxylate ligand is added that acts in competition to the bridging multidentate ligands in coordination equilibria at the metal centres and thereby controls (slows) the nucleation and growth rates. Similarly, we used various simple monodentate ligands with different chemical functionalities to prepare at room temperature ZIF-8 crystals ranging in size from ~10 nm to 1 μm.[10] The role of the various modulators could be qualitatively rationalised as modulating coordination and/or deprotonation equilibria (deprotonation of the Hmim ligand). Furthermore, we could provide direct experimental evidence by *in situ* SLS that modulators of comparatively low basicity (*e.g.* formate) act indeed as competitive ligands to retard nucleation and growth. Formate (sodium salt) was also used as a modulator to prepare big ZIF-8 macrocrystals and gas separating supported ZIF-8 membranes,[16,17] yet under solvothermal conditions using the same solvent (methanol) but a different metal salt ($ZnCl_2$ instead of $Zn(NO_3)_2\cdot 6H_2O$) and Hmim/Zn ratio (Hmim/Zn ≤ 2 instead of Hmim/Zn ≥ 4). The high-quality ZIF-8 crystals enabled

[a]*Institut für Anorganische Chemie, Leibniz Universität Hannover, Callinstr. 9, 30167 Hannover, Germany. E-mail: michael.wiebcke@acb.uni-hannover.de; Fax: +49-511-7623006; Tel: +49-511-7623698; janosch.cravillon@acb.uni-hannover.de; +49-511-7623006; +49-511-7628064*
[b]*Institut für Physikalische Chemie und Elektrochemie, Leibniz Universität Hannover, Callinstr. 3A, 30167 Hannover, Germany*
[c]*Deutsches Elektronen-Synchrotron (DESY), Notkestr. 85, 22607 Hamburg, Germany*

† Electronic supplementary information (ESI) available: Powder XRD, data of kinetic analyses, SEM micrographs, TG/DTA, and nitrogen sorption isotherm. See DOI: 10.1039/c1ce06002c

experimental determination of adsorption and diffusion data by IR microscopy and, in combination with theoretical studies using GCMC simulation methods, reliable estimation of ZIF-8 membrane permeation selectivities.[17,18]

It appeared interesting to us to investigate also the mechanism of ZIF-8 crystallisation under solvothermal conditions and clarify the role of the formate modulator (coordination or deprotonation modulation). For this purpose we performed time-resolved *in situ* energy-dispersive X-ray diffraction (EDXRD) and *ex situ* scanning electron microscopy (SEM) investigations of the synthesis with various formate concentrations and temperatures. EDXRD is a diffraction method of low *d*-spacing resolution utilising the high intensity of a synchrotron-generated white X-ray beam that can penetrate common laboratory reaction vessels and enable kinetic and mechanistic studies with high time resolution.[19] The EDXRD and SEM studies and the results are reported below.

Results and discussion

Fig. 1 shows plots of time-resolved EDXRD spectra recorded at intervals of 2 min during a ZIF-8 synthesis at 130 °C. The molar ratio of the starting solution was $ZnCl_2$/Hmim/$NaHCO_2$ (sodium formate)/MeOH = 1 : 2 : 2 : 333. Three *hkl* Bragg reflections of ZIF-8 emerge after a short induction time of $t_0 \approx$ 6 min and continuously increase in intensity, reaching a constant maximum intensity after ~100 min which corresponds to the end of the crystallisation process. Other crystalline phases were not detected, neither as intermediate phases nor as by-products. The product was pure-phase ZIF-8 as demonstrated by the high-resolution XRD pattern taken from the solid recovered after synthesis (Fig. S1, ESI†). Similarly, syntheses were monitored *in situ* (i) at different temperatures ($120 \leq T \leq 140$ °C) with constant composition (Zn/Hmim/$NaHCO_2$/MeOH = 1 : 2 : 2 : 333) and (ii) at constant temperature ($T = 130$ °C) with varying amounts of sodium formate (Zn/Hmim/$NaHCO_2$/MeOH = 1 : 2 : *x*: 333 with $0.5 \leq x \leq 4.0$). Fig. 2 shows the corresponding crystallisation curves (extent of crystallisation $\alpha(t)$ *vs.* time *t*) as obtained from the most intense 110 reflection after normalising the integrated intensities at various times to the respective integrated maximum intensities. Each synthesis yielded pure-phase ZIF-8 as demonstrated by XRD (Fig. S1, ESI†).

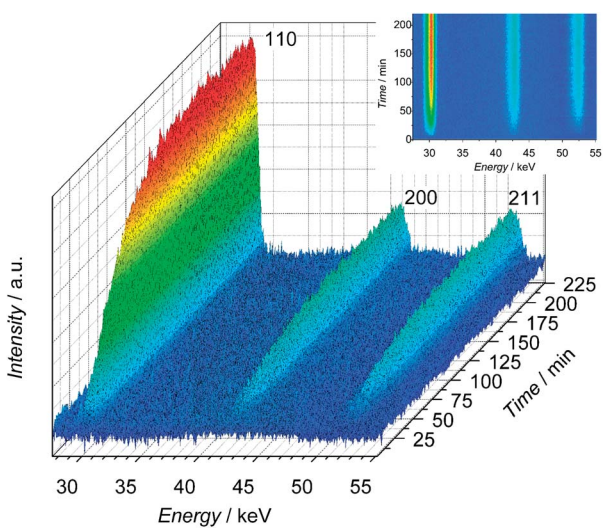

Fig. 1 Time-resolved *in situ* EDXRD spectra of ZIF-8 crystallisation at 130 °C for the composition Zn/Hmim/$NaHCO_2$/MeOH = 1 : 2 : 2 : 333.

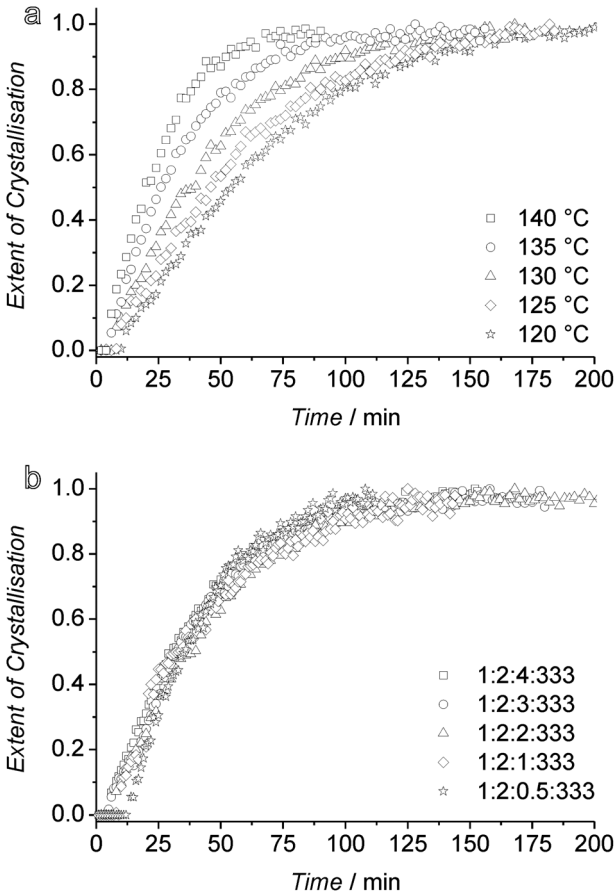

Fig. 2 Extent of crystallisation *vs.* time: (a) for the composition Zn/Hmim/$NaHCO_2$/MeOH = 1 : 2 : 2 : 333 at different temperatures as indicated and (b) for different compositions Zn/Hmim/$NaHCO_2$/MeOH = 1 : 2 : *x* : 333 ($T = 130$ °C) as indicated.

To obtain kinetic and mechanistic information, EDXRD data recorded during the solvo-/hydrothermal crystallisation of various materials,[20] including some carboxylate-based MOFs,[21–23] were most frequently evaluated applying the Avrami–Erofe'ev (abbreviated AE) equation.[24] Following that former work kinetic analysis was performed applying the method of Sharp and Hancock[25] (abbreviated SH) which is based on a linearisation of the AE equation to extract from the slope and intercept of so-called SH plots the Avrami exponent *n* and overall rate constant *k*, respectively (see Experimental section for details). Values of *n* and *k* were also determined using a non-linear least-squares procedure to fit the experimental EDXRD data with the AE equation. Fig. S2 (ESI†) shows the SH plots of the monitored syntheses, while Tables 1 and 2 list the obtained values of t_0, *n* and *k*.

Each SH plot is linear for the range $0.10 \leq \alpha(t) \leq 0.95$, indicating that mechanistic changes do not occur during a crystallisation process which is also reflected by the fits of the EDXRD data with the AE equation (Fig. S3 and S4, ESI†). The two methods of analysis yielded slightly deviating values of *n* and *k*.

Table 1 Kinetic parameters for different temperatures obtained by the Sharp–Hancock (SH) method and non-linear least-squares fitting (NLF) with the Avrami–Erofe'ev equation

T/°C	t_0/min	n_{SH}	k_{SH}/min^{-1}	n_{NLF}	k_{NLF}/min^{-1}
140	4	1.00	0.046	1.33	0.012
135	4	1.06	0.032	1.23	0.012
130	6	1.03	0.024	1.26	0.007
125	8	1.02	0.020	1.30	0.005
120	10	1.11	0.017	1.41	0.003

Table 2 Kinetic parameters for the compositions Zn/Hmim/$NaHCO_2$/MeOH = 1 : 2 : x : 333 obtained by the Sharp–Hancock (SH) method and non-linear least-squares fitting (NLF) with the Avrami–Erofe'ev equation

x	t_0/min	n_{SH}	k_{SH}/min^{-1}	n_{NLF}	k_{NLF}/min^{-1}
4.0	5	0.99	0.027	1.23	0.010
3.0	5	1.08	0.021	1.28	0.008
2.0	6	1.03	0.024	1.25	0.008
1.0	9	0.86	0.029	1.20	0.010
0.5	14	0.98	0.036	1.67	0.002

Such differences have been observed previously.[26] Nevertheless, the n values are close to 1.0 (SH analysis) or 1.3 (non-linear fitting, NLF) independent of the synthesis conditions. Values of $n \approx 1$ have been taken as an indication that crystallisation processes are rate-limited by a surface reaction[25] and it appears to be generally accepted that the importance of nucleation processes increases with increasing n. The k values increase with temperature as expected and from Arrhenius plots (Fig. S5, ESI†) the following apparent activation energies have been determined: $E_A = 66.9$ kJ mol^{-1} (k values from SH analysis) and $E_A = 113.4$ kJ mol^{-1} (k values from NLF).

As pointed out by Finney and Finke[27] a serious limitation of an AE analysis is that no differentiation is made between nucleation and growth, rather both processes are convoluted in the same parameters (n and k). Accordingly, Millange *et al.*[22] have recently successfully applied a kinetic model that separates both processes for evaluating EDXRD data of solvothermal carboxylate-based MOF crystallisations. The kinetic model was originally introduced by Gualtieri.[28] We also applied the Gualtieri model to analyse our EDXRD data (see Experimental section for details). An example of a crystallisation curve with the corresponding Gualtieri fit is shown in Fig. 3, while the remaining fitted crystallisation curves are shown in Fig. S6 and S7 (ESI†). Tables 3 and 4 list the values obtained for different parameters of the Gualtieri model which include in particular values for separate rate constants of nucleation (k_n) and growth (k_g). The model also allows extracting from the k_n values dimensionless probability curves (Gaussian function) which represent the nucleation behaviour and give some illustration on how the nucleation process extends into the growth regime (Fig. 3, S6 and S7, ESI†).

The k_n and k_g values vary only slightly with the synthesis conditions investigated. In every case k_n is smaller than k_g, suggesting that the nucleation process is rate-limiting, in contrast to what the above AE analysis indicates. The k_n and k_g values

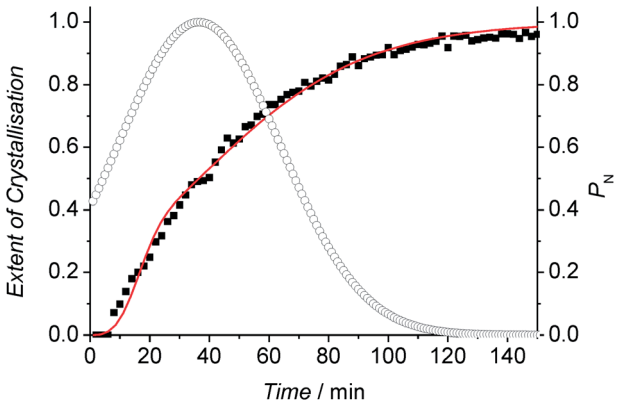

Fig. 3 Extent of crystallisation *vs.* time (black squares) for the composition Zn/Hmim/formate/MeOH = 1 : 2 : 2 : 333 (T = 130 °C) and corresponding non-linear least-squares fit with the Gualtieri equation (red curve) as well as probability curve of nucleation P_N (open circles).

Table 3 Kinetic parameters for different temperatures obtained by non-linear least-squares fitting with the Gualtieri equation

T/°C	a/min	b/min	k_g/min^{-1}	k_n/min^{-1}
140	20.6(3)	12.3(3)	0.128(6)	0.0486(8)
135	25.3(6)	21.3(6)	0.076(3)	0.0395(9)
130	36.6(7)	27.3(7)	0.059(2)	0.0274(6)
125	46.3(7)	31.9(7)	0.049(2)	0.0216(4)
120	54.7(5)	33.1(5)	0.042(1)	0.0183(2)

Table 4 Kinetic parameters for the compositions Zn/Hmim/$NaHCO_2$/MeOH = 1 : 2 : x : 333 obtained by non-linear least-squares fitting with the Gualtieri equation

x	a/min	b/min	k_g/min^{-1}	k_n/min^{-1}
4.0	30.0(5)	25.2(5)	0.066(2)	0.0333(6)
3.0	27.7(9)	29.8(7)	0.048(1)	0.036(1)
2.0	36.6(7)	27.3(7)	0.059(2)	0.0274(6)
1.0	30.6(6)	30.0(5)	0.059(1)	0.0326(7)
0.5	33.8(5)	19.9(5)	0.047(1)	0.030(1)

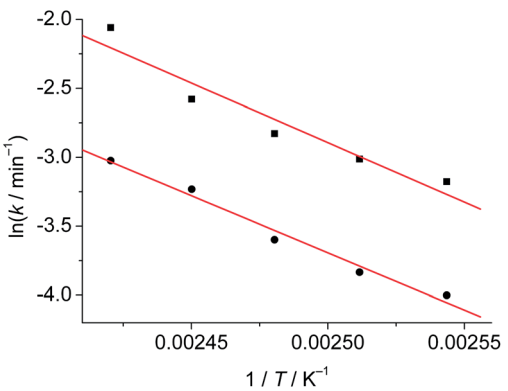

Fig. 4 Arrhenius plots for the temperature-dependent rate constants of nucleation (black circles) and growth (black squares) from the Gualtieri model.

increase with temperature and from Arrhenius plots (Fig. 4) separate activation energies and pre-exponential factors for nucleation ($E_{An} = 69.0$ kJ mol^{-1}, $A_n = 2.56 \times 10^7$ min^{-1}) and growth ($E_{Ag} = 71.8$ kJ mol^{-1}, $A_g = 1.31 \times 10^8$ min^{-1}) have been determined. The activation energies are almost equal and effects expressed by the pre-exponential factors such as collision frequencies of reactive species obviously cause the different rate constants of nucleation and growth. The kinetic parameters obtained here by the AE/SH and Gualtieri methods are comparable to those reported by Millange *et al.*[21,22] for the crystallisation of HKUST-1 ([Cu_3(btc)$_2$], btc = benzene-1,3,5-tricarboxylate) which occurred in a similar alcoholic solvent and at similar temperatures but in the absence of a modulator. However, an induction period was not observed for HKUST-1 crystallisation and the activation energies exhibit a greater difference ($E_{An} > E_{Ag}$).

An important question to be answered is the role of formate in the coordination and deprotonation equilibria during nucleation and growth of ZIF-8. The following information can be obtained from the data in Tables 2 and 4 regarding this question. First, the induction time t_0, defined as the time where the Bragg peaks were first observed, is longer for the smallest amount of formate ($x = 0.5$) than for the other amounts where t_0 values are significantly shorter. Second, the n value obtained by the non-linear fitting of the AE equation for $x = 0.5$ is larger than for the other cases. Finally, the k_n value for $x = 0.5$ is smaller than for the other cases with one exception ($x = 2.0$). Taken together, these observations suggest that formate acts to accelerate nucleation leading to a larger number of nuclei. This conclusion is further experimentally supported by the maximum size of the final crystals produced in the monitored syntheses. The maximum size decreases with increasing amount of formate because a larger number of nuclei can only grow to a smaller individual crystal size (Fig. S8 and Table S1, ESI†).

The above findings suggest that the primary role of formate is to deprotonate the bridging Hmim ligand (deprotonation modulation) and not to act as a competitive ligand (coordination modulation). In the latter case an increasing amount of formate is expected to retard nucleation and growth.[10] Further experimental evidence of the deprotonation modulation function of formate is the observation that solvothermal reactions in the absence of formate under otherwise similar conditions did not yield solid material even after prolonged periods of time (3 months). Similar observations were made recently by McCarthy *et al.*[30] during systematic synthetic work on ZIF-8 membrane fabrication. The key to successfully prepare big ZIF-8 crystals is to add only a small amount of weakly basic formate that thermodynamically drives the crystallisation process while keeping the nucleation rate low.

The deprotonation modulation function of formate is a surprising finding when considering the low basicity of a formate ion (as expressed by pK_a[HCO_2H] = 3.8 for the corresponding acid in water) compared to the basicity of a mim (deprotonated Hmim) ligand being coordinated to a Zn^{2+} ion (pK_a[Zn(Hmim)]$^{2+}$ ≈ pK_a[Zn(Him)]$^{2+}$ = 10.3 in water (Him = imidazole), data taken from the work of Kimura *et al.*).[29] Indeed, the role of formate in the present solvothermal syntheses (Hmim/Zn ≤ 2) is in contrast to its coordination modulation role in room temperature syntheses. The different behaviour of formate at room temperature may be explained with the higher Hmim/Zn ratio (≥4) which generates a high nucleation rate and formate acts to slow it.[10] However, the simple explanation based solely on the Hmim/Zn ratio neglects other possible factors such as the nature of the counter-anion (chloride *vs.* nitrate), the concentration of the reactants and the temperature.

For complementary SEM investigations solutions of the composition Zn/Hmim/$NaHCO_2$/MeOH = 1 : 2 : 2 : 333 were treated at 120 °C and quenched to room temperature in a water bath after various periods of time. The solutions were kept in the same glass tubes under similar heating conditions as for the EDXRD experiments. During the EDXRD experiments the solutions had to be stirred vigorously to avoid sedimentation of solid material out of the X-ray beam. However, SEM micrographs taken from solid material separated from stirred solutions revealed crystals with very inhomogeneous morphologies and broad size distributions and definite morphological information could hardly be obtained (Fig. S9, ESI†). It was therefore decided to continue the SEM investigations with samples taken from unstirred solutions which showed crystals with much more homogeneous morphologies. In addition, solvothermal syntheses

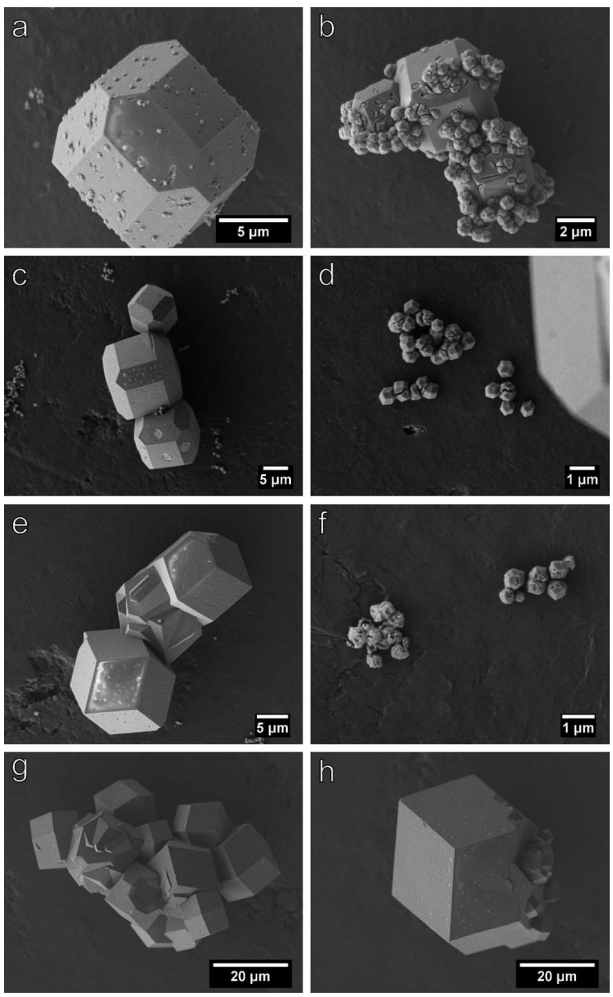

Fig. 5 SEM micrographs taken after 15 min (a and b), 20 min (c and d), 45 min (e and f) and 240 min (g and h).

are usually performed without stirring. Fig. 5 shows a series of typical SEM micrographs thus obtained.

On SEM micrographs taken after 15 min (Fig. 5a and b) comparatively large crystals together with many considerably smaller crystals are seen. Both the larger and smaller crystals exhibit the shape of a cube with truncated edges exposing 6 {100} and 12 {110} faces. The smaller crystals mostly adhere to the surfaces of the larger ones. Furthermore, indentations on the surfaces of the larger crystals can be identified that seem to be the former locations of smaller crystals which had been detached during work up. The indentations on the larger crystal's surfaces are more clearly seen on micrographs taken after 20 min (Fig. 5c and d) which still show larger and smaller crystals. The indentations indicate that the smaller crystals did not nucleate in the course of the quenching procedure, *i.e.* they are most likely not an artefact. Thus, SEM reveals that during crystal growth heterogeneous nucleation of new crystals at the surfaces of existing crystals took place. Similar heterogeneous nucleation was recently also observed during solvothermal growth of a carboxylate-based MOF (MOF-14).[21] The micrographs after 20 min also show that the larger crystals still exhibit the shape of a cube with truncated edges, while most of the smaller crystals have changed their shape to a rhombic dodecahedron exposing 12 {110} faces. After 45 min SEM micrographs (Fig. 5e and f) show that most of the larger crystals have also developed a rhombic dodecahedral shape and still exhibit indentations on the surfaces. The relative number of smaller crystals has considerably decreased and many of the smaller crystals exhibit holes, indicating that they are in a stage of dissolution. Thus, Ostwald ripening has likely taken place. After 240 min smaller crystals cannot be seen anymore (Fig. 5g, h) and all crystals have the shape of a rhombic dodecahedron, suggesting that this is the stable equilibrium morphology of ZIF-8 crystals. Fig. 6 illustrates the most probable morphology evolution during solvothermal ZIF-8 growth. It appears likely that cube-shaped crystals are formed in early stages but have a short lifetime and could therefore not be detected by SEM. An analogous sequence of morphologies was observed during modulated ZIF-8 growth at room temperature even including cubes (with rounded edges) at early stages.[10] However, heterogeneous nucleation was not observed at room temperature.

Finally, we mention that the above EDXRD studies revealed that formate modulated solvothermal crystallisation of ZIF-8 is a rapid process running to completion within <4 h. This finding allowed us to optimise our former synthesis protocols[17] with respect to efficiency (see Experimental section).

Experimental

Synthesis

An optimised formate modulated solvothermal ZIF-8 synthesis protocol is as follows: a clear solution is prepared by dissolving 30.3 mg (0.22 mmol) of $ZnCl_2$ (Sigma-Aldrich, ≥98.0%), 36.5 mg (0.44 mmol) of Hmim (Sigma-Aldrich, 99.0%) and 30.3 mg (0.44 mmol) of $NaHCO_2$ (Sigma-Aldrich, ≥99.0%) in 3 mL of MeOH (Sigma-Aldrich, ≥99.8%). The solution with a molar ratio $Zn/Hmim/NaHCO_2/MeOH = 1 : 2 : 2 : 333$ is treated without stirring at 130 °C for 4 h in a sealed glass tube under homogeneous heating in a convection oven. The crystals are recovered by filtration, washed with MeOH and dried under reduced pressure. Yield is 63% based on Zn. The rhombic dodecahedral crystals have a size up to 180 μm (Fig. 7). A thermogravimetric (TG) analysis curve (Fig. S10) and a nitrogen sorption isotherm (Fig. S11) are reported in the ESI†.

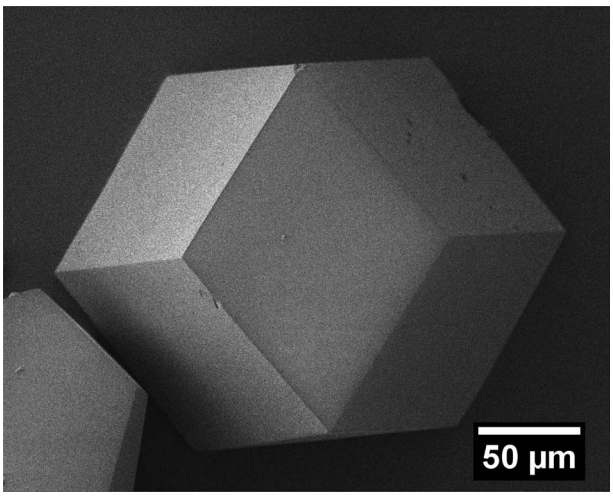

Fig. 7 SEM micrograph of a crystal from the optimised solvothermal synthesis.

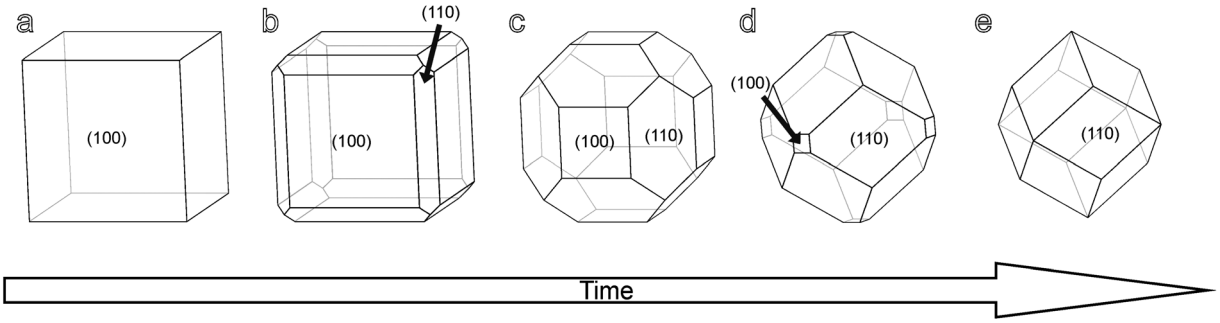

Fig. 6 Illustration of the crystal morphology evolution with time: cube (a), cube with truncated edges (b), rhombic dodecahedron with truncated corners (truncated rhombic dodecahedron) (c and d) and rhombic dodecahedron (e). Miller indices are given only for one representative face out of the different sets of symmetry-equivalent faces (crystals forms); cubic point group $\bar{4}3m$.[3]

It should be emphasised that the above homogeneous heating in a convection oven without temperature gradient deviates from the heating method used for the EDXRD and SEM investigations. In the latter cases only the lower parts ($\approx$3/4) of the glass tubes containing the synthesis solutions were heated. The temperature gradient caused refluxing of the volatile solvent (MeOH). Under these conditions smaller crystals are produced (Fig. S8†).

EDXRD investigations

Time-resolved *in situ* EDXRD experiments were performed at beam line F3 at light source DORIS III at DESY (Hamburg, Germany). The beam line receives white synchrotron radiation from a bending magnet with an energy of 8–56 keV, exhibiting a maximum photon flux at 16 keV. Diffracted radiation was recorded using a fixed angle solid-state germanium detector. The detector angle was set at $\sim$1° in order to place the most intense 110 Bragg peak of ZIF-8 close to the maximum flux of the beam. Silver behenate powder was used for detector angle calibration. Solvothermal reactions were performed in sealed borosilicate glass tubes with an inner diameter of 9 mm and a volume of 7 mL. The tubes were placed in an aluminium block that was pre-heated to the desired temperature using a circulating oil heater and equipped with a magnetic stirring device. The time between placement of the tubes and start of a diffraction experiment was $\sim$30 s. EDXRD spectra were recorded at intervals of 60 s or 120 s. The *d*-spacing (d/Å) of a Bragg peak is calculated from the recorded energy (E/keV) by

$$d = \frac{6.19921}{E \sin(\theta)} \quad (1)$$

Data were normalised to the incident beam intensity by using the logged synchrotron radiation current. The profiles of Bragg peaks were fitted with a Gaussian function.

The extent of crystallisation $\alpha(t)$ was obtained as the ratio of the integrated intensities $I(t)$ at various times to the maximum integrated intensity I_{max} at the end of the reaction by

$$\alpha(t) = \frac{I(t)}{I_{max}} \quad (2)$$

For kinetic analysis experimental EDXRD data were directly fitted with the AE equation

$$\alpha(t) = 1 - e^{-(kt)^n} \quad (3)$$

with n and k being the Avrami exponent and an overall rate constant, respectively. For SH analysis the reduced time $t_{red} = (t - t_0)$ was introduced considering the induction time t_0 and the AE equation was converted to

$$\ln[-\ln(1 - \alpha)] = n\ln(k) + n\ln(t_{red}) \quad (4)$$

The Gualtieri model considers nucleation and growth as separate processes in the following equation

$$\alpha(t) = \frac{1}{1 + e^{-(t-a)/b}}\left[1 - e^{-(k_g t)^n}\right] \quad (5)$$

with k_g and n being the rate constant and dimension of growth, respectively. We set $n = 3$ (three-dimensional growth) as proved by SEM investigations (isometric crystal shapes).

Nucleation is represented by the first term in eqn (5). From the parameters a and b the dimensionless probability of nucleation (Gaussian function) can be calculated by

$$P_N = e^{-(t-a)^2/2b^2} \quad (6)$$

with a and b being the position of the peak and the variance of the Gaussian distribution, respectively. The rate constant of nucleation is calculated by

$$k_n = \frac{1}{a} \quad (7)$$

Further methods of characterisation

High-resolution XRD patterns were recorded at room temperature using a Stoe STADI P transmission diffractometer using monochromatised $CuK_{\alpha 1}$ radiation (wavelength: 1.54060 Å). SEM micrographs were taken in secondary contrast at an acceleration voltage of 2 kV using a Jeol JSM-6700F field-emission instrument. Samples were dispersed on a carbon sample holder.

Conclusions

Using *in situ* EDXRD and *ex situ* SEM we showed that formate modulated solvothermal ZIF-8 crystallisation is a rapid process yielding big, high-quality single crystals within short time (<4 h). Analysis of crystallisation curves allowed disclosing the role of the weakly basic formate modulator. It acts as a base in deprotonation equilibria (deprotonation modulation) rather than as a competitive ligand in coordination equilibria (coordination modulation). This is in contrast to the role formate takes in room temperature ZIF-8 syntheses[10] and demonstrates that the function of simple monodentate ligands in dynamic coordination and deprotonation equilibria critically depends on a number of parameters such as basicity, complex formation constants, kind of counter-anions, ratio of metal ion to bridging ligand and temperature. It appears that coordination modulation only occurs in situations with high nucleation rates as induced, for example, by an excess of the bridging ligand,[10] rapid microwave heating[14] or low solubility of the MOF.[15] The morphology of the growing ZIF-8 crystals evolves with time in the presence of simple monodentate ligands from cubes *via* intermediate shapes to rhombic dodecahedra. The latter shape is most likely the stable equilibrium morphology of ZIF-8. The results presented here may help to put size- and shape-controlled ZIF and MOF synthesis on a more rational basis.

Acknowledgements

We thank DESY for provision of beam time at F3, Prof. W. Bensch for providing the heating device used at F3 and Beatrix Seidlhofer, Elena Antonova and Mark Freyand (Christian-Albrechts-Universität zu Kiel) for support. The work was financially supported by the DFG-SPP 1362 (Porous Metal-Organic Frameworks) organised by Prof. S. Kaskel.

Notes and references

1 A. Phan, C. J. Doonan, F. J. Uribe-Romo, C. B. Knobler, M. O'Keeffe and O. M. Yaghi, *Acc. Chem. Res.*, 2010, **43**, 58.

2 (*a*) G. Férey, *Chem. Soc. Rev.*, 2008, **37**, 191; (*b*) S. Kitagawa, R. Kitaura and S. Noro, *Angew. Chem., Int. Ed.*, 2004, **43**, 2334; (*c*) H. Furukawa, N. Ko, Y. B. Go, N. Aratani, S. B. Choi, E. Choi, A. Ö. Yazaydin, R. Q. Snurr, M. O'Keeffe, J. Kim and O. M. Yaghi, *Science*, 2010, **329**, 424.

3 (*a*) X.-C. Huang, Y.-Y. Lin, J.-P. Zhang and X.-M. Chen, *Angew. Chem., Int. Ed.*, 2006, **118**, 1587; (*b*) K. S. Park, Z. Ni, A. P. Côté, J. Y. Choi, R. Huang, F. J. Uribe-Romo, H. K. Chae, M. O'Keeffe and O. M. Yaghi, *Proc. Natl. Acad. Sci. U. S. A.*, 2006, **103**, 10186.

4 R. Banerjee, A. Phan, B. Wang, C. Knobler, H. Furukawa, M. O'Keeffe and O. M. Yaghi, *Science*, 2008, **319**, 939.

5 (*a*) Y.-S. Li, F.-Y. Liang, H. Bux, A. Feldhoff, W.-S. Yang and J. Caro, *Angew. Chem., Int. Ed.*, 2010, **49**, 548; (*b*) C. Gücüyener, J. van den Bergh, J. Gascon and F. Kapteijn, *J. Am. Chem. Soc.*, 2010, **132**, 17704; (*c*) Y. Pan and Z. Lai, *Chem. Commun.*, 2011, **47**, 10275.

6 C. Chizallet, S. Lazane, D. Bazer-Bachi, F. Bonnier, V. Lecocq, E. Soyer, A.-A. Quoineaud and N. Bats, *J. Am. Chem. Soc.*, 2010, **132**, 12365.

7 (*a*) G. Lu and J. T. Hupp, *J. Am. Chem. Soc.*, 2010, **132**, 7832; (*b*) A. Demessence, C. Boissiére, D. Grosso, P. Horcajada, C. Serre, G. Férey, G. J. A. A. Soler-Illia and C. Sanchez, *J. Mater. Chem.*, 2010, **20**, 7676.

8 (*a*) J. Cravillon, S. Münzer, S.-J. Lohmeier, A. Feldhoff, K. Huber and M. Wiebcke, *Chem. Mater.*, 2009, **21**, 1410; (*b*) Y.-S. Li, H. Bux, A. Feldhoff, G.-L. Li, W.-S. Yang and J. Caro, *Adv. Mater.*, 2010, **22**, 3322.

9 (*a*) R. E. Morris, *ChemPhysChem*, 2009, **10**, 327; (*b*) D. Zacher, R. Schmid, C. Wöll and R. A. Fischer, *Angew. Chem., Int. Ed.*, 2011, **50**, 176.

10 J. Cravillon, R. Nayuk, S. Springer, A. Feldhoff, K. Huber and M. Wiebcke, *Chem. Mater.*, 2011, **23**, 2130.

11 J. Cravillon, C. A. Schröder, R. Nayuk, J. Gummel, K. Huber and M. Wiebcke, *Angew. Chem., Int. Ed.*, 2011, **50**, 8067.

12 S. R. Venna, J. B. Jasinski and M. A. Carreon, *J. Am. Chem. Soc.*, 2010, **132**, 18030.

13 T. Tsuruoka, S. Furukawa, Y. Takashima, K. Yoshida, S. Isoda and S. Kitagawa, *Angew. Chem., Int. Ed.*, 2009, **48**, 4739.

14 S. Diring, S. Furukawa, Y. Takashima, T. Tsuruoka and S. Kitagawa, *Chem. Mater.*, 2010, **22**, 4531.

15 A. Schaate, P. Roy, A. Godt, J. Lippke, F. Waltz, M. Wiebcke and P. Behrens, *Chem.–Eur. J.*, 2011, **17**, 6643.

16 (*a*) H. Bux, F. Liang, Y. Li, J. Cravillon, M. Wiebcke and J. Caro, *J. Am. Chem. Soc.*, 2009, **131**, 16000; (*b*) H. Bux, A. Feldhoff, J. Cravillon, M. Wiebcke, Y.-S. Li and J. Caro, *Chem. Mater.*, 2011, **23**, 2262.

17 H. Bux, C. Chmelik, R. Krishna and J. Caro, *J. Membr. Sci.*, 2011, **369**, 284.

18 H. Bux, C. Chmelik, J. M. van Baten, R. Krishna and J. Caro, *Adv. Mater.*, 2010, **22**, 4741.

19 R. I. Walton and D. O'Hare, *Chem. Commun.*, 2000, **23**, 2283.

20 (*a*) R. I. Walton, T. Loiseau, D. O'Hare and G. Férey, *Chem. Mater.*, 1999, **11**, 3201; (*b*) R. I. Walton, F. Millange, D. O'Hare, A. T. Davies, G. Sankar and C. R. A. Catlow, *J. Phys. Chem. B*, 2001, **105**, 83; (*c*) L. Engelke, M. Schaefer, M. Schnur and W. Bensch, *Chem. Mater.*, 2001, **13**, 1383.

21 F. Millange, M. I. Medina, N. Guillou, G. Férey, K. M. Golden and R. I. Walton, *Angew. Chem., Int. Ed.*, 2010, **49**, 763.

22 F. Millange, R. El Osta, M. E. Medina and R. I. Walton, *CrystEngComm*, 2011, **13**, 103.

23 T. Ahnfeldt, J. Moellmer, V. Guillerm, R. Staudt, C. Serre and N. Stock, *Chem.–Eur. J.*, 2011, **17**, 6462.

24 (*a*) M. J. Avrami, *J. Chem. Phys.*, 1941, **9**, 177; (*b*) B. V. Erofe'ev, *Compt. Rend. Acad. Sci. USRR*, 1946, **52**, 511.

25 J. D. Sharp and J. H. Hancock, *J. Am. Ceram. Soc.*, 1972, **55**, 74.

26 E. E. Finney and R. G. Finke, *Chem. Mater.*, 2009, **21**, 4692.

27 E. E. Finney and R. G. Finke, *J. Colloid Interface Sci.*, 2008, **317**, 351.

28 A. F. Gualtieri, *Phys. Chem. Miner.*, 2001, **28**, 719.

29 E. Kimura, Y. Kurogi, M. Shionoya and M. Shiro, *Inorg. Chem.*, 1991, **30**, 4524.

30 M. C. McCarthy, V. Varela-Guerrero, G. V. Barnett and H.-K. Jeong, *Langmuir*, 2010, **26**, 14636.

